The Journal of Immunology

A Novel Caspase-1 Biosensor to Monitor the Progression of Inflammation In Vivo

Sarah Talley, Olga Kalinina, Michael Winek, Wonbeom Paik, Abigail R. Cannon, Francis Alonzo III, Mashkoor A. Choudhry, Katherine L. Knight and Edward M. Campbell

J Immunol published online 27 September 2019
http://www.jimmunol.org/content/early/2019/09/26/jimmunol.1900619

Supplementary Material **http://www.jimmunol.org/content/suppl/2019/09/26/jimmunol.1900619.DCSupplemental**

The Journal of Immunology is published twice each month by The American Association of Immunologists, Inc., 1451 Rockville Pike, Suite 650, Rockville, MD 20852

Print ISSN: 0022-1767 Online ISSN: 1550-6606.

Published September 27, 2019, doi:10.4049/jimmunol.1900619

A Novel Caspase-1 Biosensor to Monitor the Progression of Inflammation In Vivo

Sarah Talley,* Olga Kalinina,† Michael Winek,‡ Wonbeom Paik,† Abigail R. Cannon,* Francis Alonzo, III,† Mashkoor A. Choudhry,* Katherine L. Knight,† and Edward M. Campbell*,†,‡

Inflammasomes are multiprotein complexes that coordinate cellular inflammatory responses and mediate host defense. Following recognition of pathogens and danger signals, inflammasomes assemble and recruit and activate caspase-1, the cysteine protease that cleaves numerous downstream targets, including pro–IL-1β and pro–IL-18 into their biologically active form. In this study, we sought to develop a biosensor that would allow us to monitor the initiation, progression, and resolution of inflammation in living animals. To this end, we inserted a known caspase-1 target sequence into a circularly permuted luciferase construct that becomes bioluminescent upon protease cleavage. This biosensor was activated in response to various inflammatory stimuli in human monocytic cell lines and murine bone marrow–derived macrophages. Next, we generated C57BL/6 transgenic mice constitutively expressing the caspase-1 biosensor. We were able to monitor the spatiotemporal dynamics of caspase-1 activation and onset of inflammation in individual animals in the context of a systemic bacterial infection, colitis, and acute graft-versus-host disease. These data established a model whereby the development and progression of inflammatory responses can be monitored in the context of these and other mouse models of disease. ***The Journal of Immunology*****, 2019, 203: 000–000.**

Numerous cell types, canonically cells of the innate immune system, express cytosolic, nuclear, and membrane-associated pattern recognition receptors (PRRs), which are able to sense general danger signals, pathogen-associated molecular patterns (PAMPs), and damage-associated molecular patterns (DAMPs). PRRs then activate signaling cascades to coordinate the appropriate immune response necessary for pathogen clearance. A subgroup of cytosolic PRRs in the Nod-like receptor (NLR) family and absent in melanoma 2 (AIM2)–like receptor are capable of forming multiprotein complexes called inflammasomes (1–11). Following recognition of their cognate ligand, NLR and AIM2 recruit the adaptor protein apoptosis-associated speck-like protein containing a CARD (ASC), which oligomerizes into filamentous complexes, providing a platform for the recruitment and subsequent activation of caspase-1 (1–4, 8, 10–15). In addition to the NLR and AIM2 family of proteins, other proteins such as Pyrin, IFI16, and RIG-I also form functional inflammasomes in response to various pathogens or danger signals (1, 5, 11, 16–18). As such, a myriad of PAMPs and DAMPs drive the formation of multiple different inflammasomes, all of which culminate in the proteolytic activation of caspase-1. Once activated, caspase-1 cleaves numerous downstream targets, such as the proinflammatory cytokines pro–IL-1β and pro–IL-18, leading to their maturation and secretion from cells. The processing and release of these cytokines and other inflammatory effectors activates immune cells to initiate inflammatory responses. Although inflammation is important for mounting immune responses, the timely resolution of inflammation is necessary to prevent tissue damage following pathogen clearance. Maintaining immune homeostasis is critical to host health, as dysregulation of these inflammatory pathways underlines the pathology of numerous diseases, including neurodegenerative diseases, intestinal disorders, obesity, allergy, arthritis, diabetes, pulmonary diseases, cancer, and many autoimmune disorders (3, 9, 11, 15, 19, 20).

Despite the central role inflammation plays in infections and human diseases, the conventional methods used to measure inflammation have significant limitations, especially in vivo. The primary methods used to detect inflammasome activation are the proteolytic cleavage of pro–caspase-1 to caspase-1 by immunoblot or secretion of IL-1β in the serum by ELISA, both of which have notable limitations. Measuring the proteolytic cleavage of caspase-1 by immunoblot requires tissue removal from sacrificed animals, preventing the dynamic measurement of caspase-1 in individual animals over time. Furthermore, modest and/or transient activation of caspase-1 can induce very consequential levels of inflammation while being difficult or impossible to detect by Western blot analysis of tissue homogenates. Similarly, some models of disease are associated with inflammatory responses sufficient to allow detection of IL-1β in the bloodstream, but this

*Department of Integrative Cell Biology, Stritch School of Medicine, Loyola University Chicago, Maywood, IL 60153; †Department of Microbiology and Immunology, Stritch School of Medicine, Loyola University Chicago, Maywood, IL 60153; and ‡Department of Neuroscience, Stritch School of Medicine, Loyola University Chicago, Maywood, IL 60153

ORCIDs: 0000-0002-8620-2046 (M.W.); 0000-0001-8048-5383 (W.P.); 0000-0003-2108-9457 (K.L.K.).

Received for publication May 30, 2019. Accepted for publication August 21, 2019.

K.L.K. was supported by National Institute of Allergy and Infectious Diseases (NIAID)/National Institutes of Health Grant AI10586. M.A.C. was supported by National Institute on Alcohol Abuse and Alcoholism (NIAAA) Grant R21AA025806. A.R.C. was supported by NIAAA Grant T32AA013527. S.T. was supported by NIAID Grant T32AI007508. E.M.C. was supported by a Distinguished Investigator Award from the Emerald Foundation.

Address correspondence and reprint requests to Dr. Edward M. Campbell, Loyola University Chicago, 2160 South First Avenue, Maywood, IL 60153. E-mail address: ecampbell@luc.edu

The online version of this article contains supplemental material.

Abbreviations used in this article: ASC, apoptosis-associated speck-like protein containing a CARD; BMDM, bone marrow–derived macrophage; CBA, cytometric bead array; DAMP, damage-associated molecular pattern; DSS, dextran sodium sulfate; GVHD, graft-versus-host disease; LDH, lactate dehydrogenase; NLR, Nod-like receptor; NT, no treatment; PAMP, pathogen-associated molecular pattern; PRR, pattern recognition receptor; WT, wild-type.

is often not the case, especially when inflammation is localized to specific tissues. Moreover, even when IL-1β can be detected in the bloodstream, this assay gives no insight regarding the tissue or cells producing IL-1β. The inability to identify locations within tissues where caspase-1 activation is occurring adds significant limitations to both of these assays and makes them inherently qualitative, rather than quantitative.

In this study, we developed a biosensor that directly monitors caspase-1 activation, which allows us to monitor the kinetics and magnitude of inflammatory responses in living animals over time. We used a circularly permuted luciferase construct that is activated upon proteolytic cleavage (21, 22) and identified a biosensor that was strongly activated by caspase-1 in 293T cells. This biosensor was also activated in response to stimuli that trigger NLRP3 and AIM2 inflammasomes in THP-1 cells and murine bone marrow–derived macrophages (BMDMs). Transgenic mice expressing this sensor were generated and used to monitor inflammatory responses occurring in three animal models of disease. In models of a systemic bacterial infection, dextran sodium sulfate (DSS)–induced colitis and acute graft-versus-host disease (GVHD), biosensor activation was observed in biologically relevant tissues and cell types and correlated with expected pathological outcomes and established inflammatory indices. These data indicate that this biosensor can be a valuable means to monitor and measure cellular inflammatory responses in living animals throughout disease progression.

Materials and Methods

Cell culture

HEK293T and THP-1 cells were obtained from the American Type Culture Collection. Cells were cultured at 37˚C in 5% CO_2 in DMEM or RPMI 1640, respectively, supplemented with 10% FBS (Life Technologies) with 100 U/ml penicillin, 100 U/ml streptomycin, and 10 μg/ml ciprofloxacin. THP-1 cells were treated with 100 ng/ml PMA for 48 h for differentiation into macrophages. BMDMs were isolated as previously described (23). Cells were cultured in DMEM high glucose (Hyclone) with 10% characterized FBS (Life Technologies), 1× nonessential amino acids (Life Technologies), 1× HEPES buffer (Hyclone), 100 U/ml penicillin, 100 U/ml streptomycin, and 20 ng/ml M-CSF (PeproTech).

293T transfections and luciferase reporter assay

HEK293T cells were plated at ∼70% confluence in 100 μl DMEM in a 96-well black wall, clear bottom plate (Corning). Cells were allowed to adhere to the wells for 3 h. Cells were transfected with a pGLO sensor construct containing the target sequence in pro–caspase-7 and ASC and pro–caspase-1 expression plasmids. Medium was replaced with CO_2 independent medium supplemented with 10% FBS (Life Technologies) only and allowed to equilibrate for 2 h prior to addition of GloSensor reagent (Promega).

Generation of stable cell lines

Caspase-1 biosensors containing the IQAD amino acid target sequence was synthesized (Integrated DNA Technologies) and cloned into pLVX (XhoI and EcoRI). Lentiviral vectors were generated by transfecting HEK293T with equal ratio of pLVX–IQAD, psPAX2 packaging construct (from Dr. D. Trono, catalog no. 11348; National Institutes of Health AIDS Reagent Program), and vesicular stomatitis virus glycoprotein (VSVg) using polyethylenimine (PEI; Polysciences). After 48 h, supernatant was harvested, filtered through a 0.45-μM filter (MilliporeSigma), and added to cells. Cells were transduced by spinoculation (1200 g, 2 h at 13˚C) (24). After 48 h, the medium was replaced with medium containing 5 μg/ml puromycin.

In vitro inflammasome activation assays

Differentiated THP-1 cells or BMDMs were plated in 48-well or 24-well plates and stimulated with the indicated stimuli. Cells were primed with 10 ng/ml LPS (from *Escherichia coli* 055:B5; Sigma-Aldrich) for 4 h, followed by 5 mM ATP (InvivoGen) for 30 m or 1 h. Supernatant and cells were harvested at the indicated time points for ELISA, immunoblot, and luciferase assays. Alternatively cells were transfected with 10 μg/ml poly(dA:dT) (Sigma-Aldrich) or 100 μg/ml poly(I:C) (Sigma-Aldrich) with Lipofectamine in medium without antibiotics. Six hours later, supernatant and cells were harvested for ELISA and luciferase assays. For caspase-1 inhibitor experiments, THP-1 cells were treated with Z-WEHD-FMK (R&D Systems) or DMSO control for 1 h prior to LPS stimulation. For in vitro luciferase measurements, cells were lysed in 1× passive lysis buffer (Promega). Lysates were plated in duplicate or triplicate in 96-well plates. Firefly luciferase substrate (Promega) was added to each well, and luminescence (relative light units) was quantified. IL-1β ELISA was performed according to the manufacturer's instructions (RayBiotech). Cytometric bead array (CBA) (BD Biosciences) was performed according to the manufacturer's instructions, and samples were analyzed on an LSRFortessa. The $\log_2$ fold change was calculated for each treatment group and heatmaps were generated using RStudio.

Western blotting

For detection of caspase-1 in the supernatant, proteins were concentrated from 500 μl of supernatant by methanol/chloroform precipitation. Protein pellets were suspended in Nonidet P-40 lysis buffer (100 mM Tris, pH 8, 1% Nonidet P-40, 150 mM NaCl) containing a protease inhibitor mixture (Roche), and protein concentration was quantified by BCA (Pierce; Thermo Fisher Scientific). For detection of proteins in tissues, tissues were homogenized in lysis buffer with protease inhibitor mixture, and homogenates were shaken on ice for 30 min. Homogenates were centrifuged at 3900 rpm for 10 min, lysates were collected, and protein concentration was quantified as above. Proteins were mixed with 2× Laemmli sample buffer and boiled at 100˚C for 5 min. Equal concentrations of proteins were loaded onto a 4–15% gradient gel (Bio-Rad) and transferred to a nitrocellulose membrane (Bio-Rad). Membranes were incubated with anti–caspase-1 (Adipogen) or anti–β-actin (Santa Cruz Biotechnology), followed by anti-mouse IgG conjugated to HRP (Thermo Fischer Scientific). Ab complexes were detected using Super-Signal West Femto Chemiluminescent Substrate (Thermo Fisher Scientific), and chemiluminescence was measured in a FluorChem E machine (ProteinSimple).

Generation of caspase-1 biosensor transgenic mice

Caspase-1 biosensors containing the IQAD target sequence were synthesized (Integrated DNA Technologies) and cloned into the EcoRI and XhoI sites of pCAG. SalI and HindIII digested DNA containing the CAG promoter and intron, caspase-1 biosensor, and polyA sequence was purified and microinjected into zygotes of C57BL/6 mice (performed by Northwestern Transgenic and Targeted Mutagenesis Laboratory). Progeny were genotyped by PCR of the tail DNA, and transgene-positive mice were identified. The founder line that exhibited ubiquitous and robust transgene expression in all tissues was expanded. For transgene expression quantification, mouse tissues were homogenized, and RNA was isolated (NucleoSpin RNA Plus; Macherey-Nagel) and converted to cDNA (GoScript Reverse Transcription System; Promega). Transgene or mouse β-actin expression was quantified by quantitative RT-PCR using SYBR Green (Bio-Rad). Caspase-1 biosensor mice are maintained as heterozygote. All experiments were performed according to protocols approved by the Institutional Animal Care and Use Committee at Loyola University Chicago. All animals were housed in pathogen-free conditions at Loyola University Chicago medical campus (Maywood, IL); animals used for *Staphylococcus aureus* experiments were housed in a BSL-2 facility at Loyola University Chicago medical campus (Maywood, IL).

Lactate dehydrogenase measurements

Lactate dehydrogenase (LDH) cytotoxicity assay was performed according to the manufacturer's instructions (Pierce; Thermo Fisher Scientific). Briefly, supernatants were collected and centrifuged to remove cell debris. Maximum LDH activity was determined in supernatant from cells incubated with 10× Lysis Buffer. Background LDH activity present in the serum was measured using culture medium.

IVIS imaging

Mice were anesthetized using 2% isoflurane/air mixture delivered by the Xenogen IVIS Spectrum XGl-8 Gas Anesthesia system and injected i.p. or i.v. with a single dose of 150 mg/kg VivoGlo Luciferin for in vivo bioluminescence imaging. Anesthetized mice were placed in the IVIS imaging chamber and imaged with the IVIS 100 Imaging System (Xenogen) 10 min after i.p. administration of the luciferase substrate or immediately following i.v. administration of the substrate. Bioluminescence was quantified and analyzed use Living Image software.

S. aureus *culture and murine systemic infection model*

Caspase-1 biosensor mice were infected with 10^7 CFU *S. aureus* as described previously (25–27). Briefly, *S. aureus* (USA300 strain LAC) cultures were grown in tryptic soy broth overnight at 37°C and subcultured 1:100 in fresh tryptic soy broth at 37°C for 3 h. Cultures were centrifuged, and bacterial pellets were washed in PBS and normalized to an inoculum of 10^8 CFU/ml. Mice were anesthetized via i.p. injection with 250 mg/kg Avertin and infected via the retro-orbital plexus with 100 μl PBS containing 10^7 CFU *S. aureus*. Tissues were isolated from infected animals and homogenized using an electric homogenizer. CFU was enumerated by plating tissue homogenates on tryptic soy agar plates for 16 h at 37°C. Tissue homogenates were centrifuged at 3900 rpm for 10 min, and supernatant was collected for CBA analysis using BD CBA Flex sets and mouse inflammation kit (BD Biosciences).

DSS-induced colitis model

Caspase-1 biosensor mice were exposed to DSS as described previously (28). Briefly, mice were given molecular grade water with or without 2% DSS (40,000 kDa; MP Biomedicals) for 5 d. For female mice, DSS treatment was extended 48 h and DSS concentration was doubled to 4% for the final 24 h. Mice were weighed daily throughout the course of the experiment. On day 5 or 7, mice were injected with luciferase substrate and sacrificed 10 min later. Colons were excised and bioluminescence was measured ex vivo. Colon length was measured and fecal samples were assessed for blood using a Hemoccult test (Beckman Coulter). Tissue sections were fixed in 10% phosphate buffered formalin, paraffin embedded, processed, and stained with H&E by AML laboratories (Saint Augustine, FL) or homogenized and used for Western blot analysis of caspase-1 activation. Colon samples were weighed and homogenized and 5 μl of homogenates were used for CBA (BD Biosciences).

GVHD model

On day 0, wild-type (WT) BALB/c mice were irradiated. Caspase-1 biosensor mice were sacrificed and bone marrow cells were harvested as described above. For splenocyte isolation, spleens were pressed through a sterile 100-μm cell strainer. The cell strainer was flushed with medium to dislodge the cells. Cells were centrifuged for 5 min, and pellets were resuspended in ACK lysis buffer (Life Technologies) and washed with medium. Splenocytes and bone marrow cells were counted and resuspended in 300 μl PBS. T cells were purified (≥90% purity, confirmed by flow cytometric analysis of CD3 expression on purified splenocytes) from total splenocytes by negative selection, using biotin anti-mouse B220 (RA3-6B2), biotin anti-mouse CD11b (M1/70) and biotin anti-mouse CD11c (N418), followed by incubation with magnetic nanoparticles conjugated to streptavidin (BD IMag Streptavidin Particles Plus; BD Biosciences). Heparin was added prior to i.v. injection. Bone marrow cells (10^7) with or without 5×10^6 splenocytes or bone marrow cells with $1.3–1.5 \times 10^6$ T cells were injected into recipient mice. All donor and recipients were sex matched. Serum was collected from mice on day 7, and cytokine levels were assessed by CBA (BD Biosciences). Clinical scores were obtained by three independent researchers. Mice were given a score of 0–2 (2 being most severe) in each of the following categories: activity, posture, fur texture/grooming. Scores were totaled for each mouse. Weight loss was measured separately and was not included in the clinical score. Percentage of donor $CD8^+$ and $CD4^+$ T cells and their activation status was analyzed by flow cytometry. All Abs were obtained from BioLegend (anti-H-2Kd [SF11.1], anti-CD45.1 [A20], anti-CD4 [GK1.5], anti-CD8a [53-6.7], anti-CD44 [IM7], anti-CD25 [PC61], anti-CD69 [H1.23F]).

Statistical analysis

Statistical significance was assessed using GraphPad Prism software (GraphPad Software). Student *t* test was employed when comparing a treatment group relative to those receiving no treatment (NT). One-way ANOVA was performed when comparing a group of data, followed by either a Tukey post hoc test or Dunnett multiple comparison test to determine significance. Data are represented as mean ± SEM or SD, and $p < 0.05$ was considered significant.

Results

Generation of caspase-1 biosensors

To better monitor inflammatory responses in various disease settings, we sought to develop a bioluminescent sensor that detects caspase-1 activation. We employed a circularly permuted form of luciferase, in which the N- and C-terminal domains necessary for bioluminescence are physically separated by a flexible hinge region (21). A caspase-1 target sequence found in pro–caspase-7 (hereafter referred to as IQAD) (29–32) was cloned into this linker region, with the expectation that upon caspase-1 activation, this sequence would be cleaved, allowing the two domains of luciferase to associate (Fig. 1A). This results in a strong gain in luciferase activity, so that the degree to which caspase-1 is activated can be quantified. We tested the ability of this biosensor to measure caspase-1 activation by transiently expressing our construct in HEK293T cells. To reconstitute an inflammasome pathway in these cells, we additionally cotransfected pro–caspase-1 and ASC (33, 34) or a GFP sham, and luminescence was measured in living cells. We detected robust activation of a biosensor containing the IQAD caspase-1 target sequence (Fig. 1B). To evaluate the utility of this biosensors in a more biologically relevant setting, we transduced human monocytic THP-1 cells with lentiviral vectors expressing our IQAD biosensor. Cells were differentiated with PMA, then stimulated with LPS and ATP to activate the NLRP3 inflammasome. This treatment resulted in a significant increase in luminescence and IL-1β secretion relative to untreated control cells, indicating that the IQAD biosensor is activated in response to inflammatory stimuli in vitro (Fig. 1C, 1D). On average, we found ∼20-fold induction in luciferase signal in response to LPS and ATP, although this number varied between experiments ranging from ∼2–3-fold (low) to ∼50-fold (high) relative light units relative to untreated cells (Supplemental Fig. 1A). To confirm that the IQAD biosensor signal quantitatively reports caspase-1 activation, cells were treated with the caspase-1 inhibitor Z-WEHD-FMK and stimulated with LPS and ATP. We found a dose-dependent decrease in biosensor activation in the presence of increasing concentrations of caspase-1 inhibitor (Supplemental Fig. 1B). We did not detect significant LDH activity in the supernatant of LPS and ATP-stimulated cells, compared with control, indicating that the IQAD biosensor is activated in living cells (Supplemental Fig. 1C). We also transfected IQAD cells with synthetic dsDNA poly(dA:dT) or dsRNA poly(I:C), as cytosolic DNA and RNA triggers caspase-1 activation through the AIM2 and NLRP3 inflammasomes, respectively (35–37). We observed robust IQAD biosensor activation in response to both poly(dA:dT) and poly(I:C) (Fig. 1E).

Generation of caspase-1 IQAD reporter mice

Transgenic mice expressing the IQAD biosensor were generated by microinjection of a transgene containing the biosensor under control of the chicken β-actin promoter and CMV early enhancer for ubiquitous transgene expression (38–40) (Supplemental Fig. 2A). The transgene was purified and microinjected into zygotes of C57BL/6 mice (Supplemental Fig. 2B). Offspring were genotyped by PCR of the tail DNA to identify positive founders. Four founder lines were initially identified (Supplemental Fig. 2C), one of which successfully delivered positive progeny that exhibited ubiquitous transgene expression in all tissues (Supplemental Fig. 2D). To determine if the IQAD biosensor was functioning in these transgenic mice, BMDMs from IQAD mice were treated with a panel of inflammatory stimuli, and the luciferase signal generated from proteolytic cleavage of caspase-1 and IL-1β secretion were measured. As expected, biosensor activation and IL-1β secretion were detected in BMDMs stimulated with LPS and ATP (Fig. 2A, 2B), and activated caspase-1 was detected in the supernatant of LPS and ATP-stimulated BMDMs by Western blot analysis (Fig. 2C). We also measured robust biosensor activation in BMDMs transfected with poly(dA:dT) and poly(I:C) (Fig. 2D). We did detect cytotoxicity in response to some inflammatory stimuli, including poly(dA:dT), which is known to induce pyroptosis, and poly(I:C), whereas no

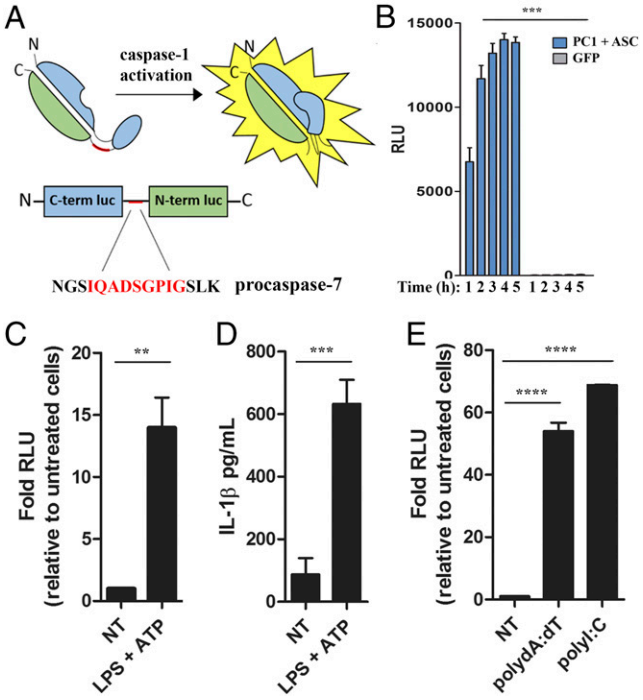

FIGURE 1. Caspase-1 biosensors are activated in response to inflammatory stimuli in vitro. Schematic representation of caspase-1 biosensor design (**A**). The IQAD biosensor was transfected into 293T cells in the presence of pro–caspase-1 (PC1) and ASC expression plasmids or a GFP sham control plasmid. Thirty-six hours later, a live cell luciferase substrate (GloSensor cAMP reagent; Promega) was added to cells, and luciferase reads were taken 1–5 h after addition of the substrate (**B**). THP-1 cells stably expressing the IQAD biosensor were differentiated with PMA, then stimulated with LPS for 4 h followed by ATP for 30 min. Three hours later, cells were lysed and luciferase activity was quantified (**C**). Supernatant from IQAD THP-1 cells treated with or without LPS and ATP was harvested, and IL-1β levels were measured by ELISA (**D**). IQAD THP-1 cells were transfected with poly(dA:dT) or poly(I:C); luciferase activity was quantified 6 h later (**E**). Data shown are representative of at least three independent experiments, displayed as mean ± SD (B and D) or fold change of the means relative to the mean of the NT group ± SD (C and E). $***p < 0.0001$ by ANOVA followed by Tukey post hoc test comparing each column to its respective time point (B), $**p \leq 0.005$, $***p \leq 0.0005$, $****p < 0.0001$ by unpaired two-tailed *t* test (C–E).

cell death was detected in cells treated with LPS and ATP (Fig. 2E). We also performed CBA to assess cytokine and chemokine secretion in parallel with biosensor activation. In addition to IL-1β, LPS-primed cells treated with ATP secreted a panel of inflammatory cytokines, including IL-1α, IL-6, and TNF as well as the chemokines keratinocyte chemoattractant CXCL1, MCP-1, MIP (MIP-1α, MIP-1β), and RANTES (CCL5) (Fig. 2F). Together, these data suggest that caspase-1 biosensors are activated in cells undergoing inflammatory responses.

IQAD biosensors are activated and secreted in response to apoptotic stimuli

Although the IQAD recognition sequence in pro–caspase-7 is a well-established target of caspase-1 in vitro and in vivo (29–31), pro–caspase-7 is also activated by initiator caspases caspase-8, -9, and -10 during apoptosis (29). To determine if the IQAD biosensor was activated in cells in response to apoptotic stimuli, THP-1 cells were treated with staurosporine, and biosensor activation was quantified. Although we measured significant biosensor activation in cell lysates following LPS and ATP treatment, we observed minimal biosensor activation in lysates following staurosporine treatment (Supplemental Fig. 3A). However, we did observe significant biosensor activation in the supernatant of staurosporine-treated cells, whereas we did not observe a similar increase in the supernatant of cells treated with LPS and ATP (Supplemental Fig. 3A). These data suggest that although the IQAD biosensor can be activated in response to apoptotic stimuli, it is released from apoptotic cells and retained in cells following inflammasome activation. We next examined biosensor activation in internal organs, including the thymus, which is known to have constitutively high levels of apoptosis due to ongoing negative selection of developing T cells. When the thymus was excised from positive transgenic mice and bioluminescence was measured, we observed minimal biosensor activation in the thymus ex vivo, relative to other tissues isolated (Supplemental Fig. 3B, 3C). Thus, although the IQAD biosensor is activated by apoptotic stimuli in vitro, its ability to serve as a biosensor of apoptosis in vivo is poor, potentially because of degradation of the biosensor in the extracellular environment or the rapid clearance of apoptotic cells in vivo (41, 42).

Monitoring biosensor activation during S. aureus *systemic infection*

To determine if caspase-1 biosensors could be used to monitor inflammatory responses in vivo, we chose a systemic *S. aureus* infection model. This Gram-positive bacterium is typically found as a commensal but can become pathogenic, causing local skin infections or more serious systemic illness, accompanied by bacteremia, abscess formation in tissues, endocarditis, and morbidity and mortality (43). The bacterium encodes a number of virulence factors that potently stimulate inflammatory responses (44, 45). *S. aureus* infection triggers PRRs and subsequent production of inflammatory cytokines and chemokines, leading to the recruitment of neutrophils and abscess formation in tissues (46). Specifically, many components of the bacterial wall and pore-forming toxins are capable of providing signal 1 via TLR2 activation and signal 2, driving inflammasome activation (44, 46, 47). Multiple inflammasomes are known to be triggered by *S. aureus*, mainly NLRP3 (47–51). Importantly, caspase-1 is critical, as caspase-1–deficient macrophages are impaired in cytokine production (52). To test the IQAD biosensor in vivo, we used a model of *S. aureus* infection in the bloodstream, which induces systemic inflammation in mice. IQAD mice were infected with *S. aureus* (or PBS control) via retro-orbital injection, and luminescence was quantified 0, 1, 2, and 3 d postinfection using an IVIS imaging system (Fig. 3A). For imaging, mice were injected i.p. with 150 mg/kg VivoGlo Luciferin, a luciferase substrate designed for measuring luciferase in live animal studies. Relative to the background biosensor signal measured on day 0, the infected mice exhibited increased biosensor activation over the course of infection (Fig. 3A). On day 3, infected and control mice were sacrificed following in vivo imaging, and the bioluminescence of individual organs was quantified ex vivo (Fig. 3B). We detected increased luciferase signal in the livers, kidneys, hearts, and spleens isolated from *S. aureus*–infected mice, whereas little to no biosensor activation was detected in tissues isolated from the PBS controls (Fig. 3B, 3C, data not shown). Notably, we measured cleaved caspase-1 in infected tissues in which we detected high levels of biosensor activation (Fig. 3D). Bacterial CFU and cytokine expression were also quantified to determine if bacterial burden and/or inflammatory markers coincided with areas of bioluminescence. We detected bacterial colonization in all kidneys and livers isolated from infected mice, consistent with the increased biosensor activation detected in these tissues (Fig. 3E). Bacteria were detected in the heart and spleen of some, but not all,

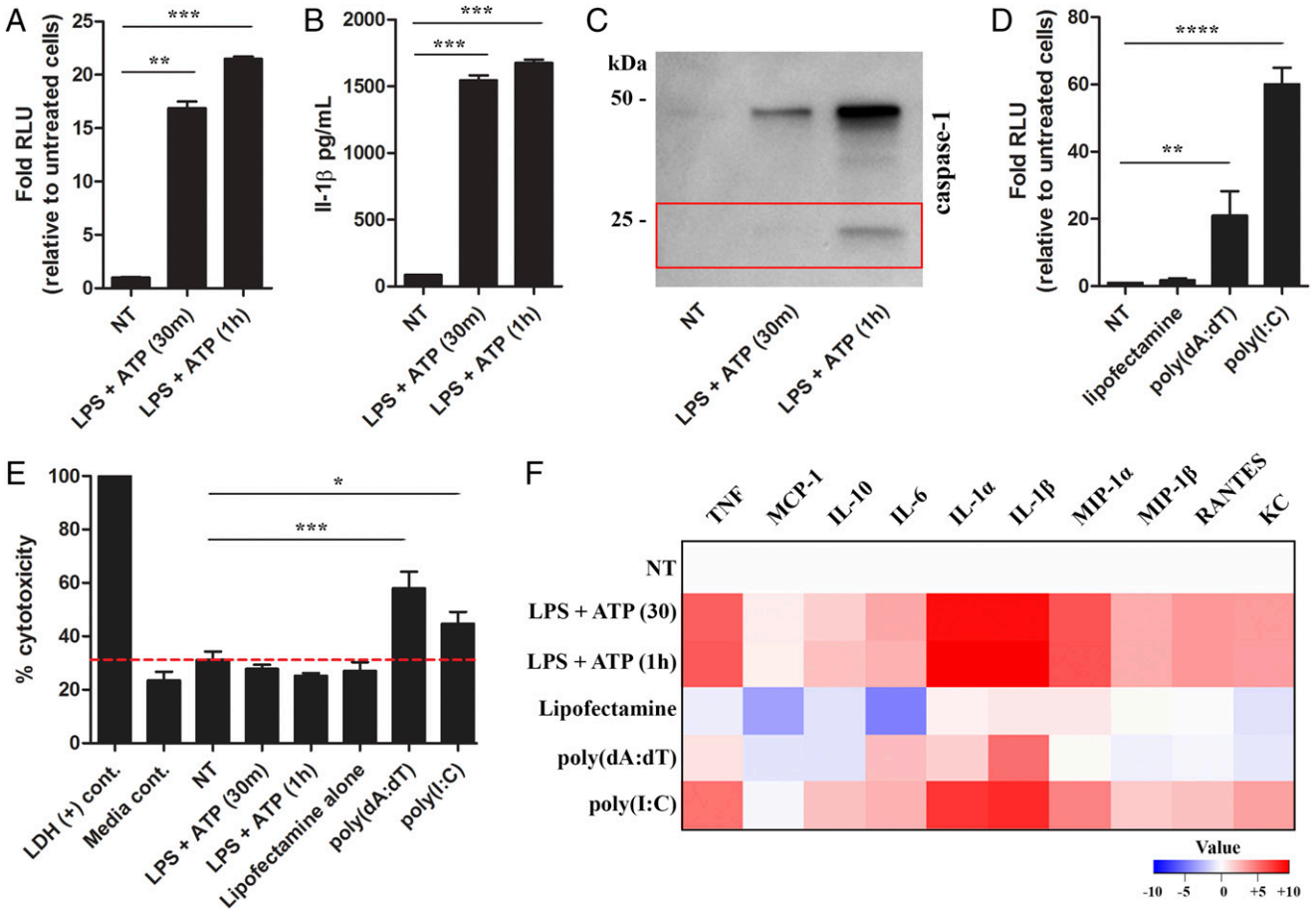

FIGURE 2. Caspase-1 biosensors are activated in BMDMs. BMDMs from IQAD biosensor mice were treated with 10 ng/ml LPS for 4 h, followed by 5 mM ATP for 30 m or 1 h. Luminescence was quantified from cells (**A**), IL-1β levels were quantified in the supernatant by ELISA (**B**), and caspase-1 activation was measured in the supernatant by Western blot (**C**). BMDMs from IQAD biosensor mice were transfected with poly(I:C) or poly(dA:dT) for 6 h, and luminescence was quantified (**D**). LDH and CBA analysis of supernatants from cells stimulated with the indicated treatment (**E** and **F**). LDH activity is normalized to the LDH maximum control (100% cytotoxicity), with the red dashed line representing the average LDH activity in unstimulated BMDMs (E). The $\log_2$ fold change relative to the NT group was calculated and plotted as a heatmap, where each cytokine/chemokine is displayed on the *x*-axis (F). Data shown are representative of at least three independent experiments from different donor IQAD mice, displayed as fold change of the means relative to the mean of the NT group ± SD (A and D), mean ± SD (B), or the mean percentage cytotoxicity across $n = 3$ experiments, mean ± SEM (E). $^{*}p \leq 0.05$, $^{**}p \leq 0.005$, $^{***}p \leq 0.0005$, $^{****}p < 0.0001$ by unpaired two-tailed *t* test (A, B, and D) or by ANOVA followed by Dunnett multiple comparison test comparing each column to the control NT column (E).

infected mice (data not shown). We also found increased expression of a panel of inflammatory cytokines and chemokines in tissues and serum isolated from infected mice, relative to uninfected controls (Fig. 3F, 3G, data not shown). These data demonstrate that caspase-1 biosensors are activated in vivo in response to *S. aureus* infection and that we can monitor changes in biosensor activation over the course of disease in living animals and in infected tissues ex vivo.

Monitoring biosensor activation during colitis

We next sought to measure biosensor activation in the context of intestinal inflammation using an established model of DSS-induced ulcerative colitis (28). We chose this model because, in the absence of caspase-1, DSS-induced colitis is alleviated, indicating that caspase-1 activation is essential for intestinal inflammation (53–55). Mice were treated with 2% DSS (or PBS control) ad libitum in the drinking water for 5 d to induce acute colitis in animals. Female mice did not exhibit colitis symptoms at this dose and time point, so they were given an extra 48 h of DSS treatment with a boost of 4% DSS the final 24 h of the experiment, consistent with the idea that male mice are more susceptible to DSS-induced colitis (56, 57). On day 5 or 7, mice were weighed, injected with the luciferase substrate, and sacrificed. Colons were extracted and bioluminescence was measured ex vivo. We found biosensor activation in colons isolated from DSS-treated mice on day 5 in males and day 7 in females (Fig. 4A). During colitis, inflammation starts distally and becomes more proximal as disease progresses. The detection of strong biosensor activation in the distal colon is consist with this progression and demonstrates the ability of this biosensor to monitor inflammation relevant to this disease model. Areas where we detected biosensor activation and control regions that did not exhibit bioluminescence were sectioned and stained with H&E for histopathological assessment. In tissue sections derived from areas of biosensor activation, we found nodules with inflammatory infiltrate in the mucosa and submucosa regions of the colon, as well as a loss of crypt integrity, reduction of goblet cells, disruption of the epithelial barrier, neutrophil infiltration, edema, and thickening of the muscularis mucosae (Fig. 4A, 4B). None of these inflammatory hallmarks were found in control sections from the same mice, although we did find crypt elongation in some proximal sections where no bioluminescence was detected (Fig. 4A, 4B, 14P). Notably, we detected biosensor activation that corresponded with histopathology even in mice that did not show extensive symptoms of disease such as weight loss, colonic shortening, and blood in the stool

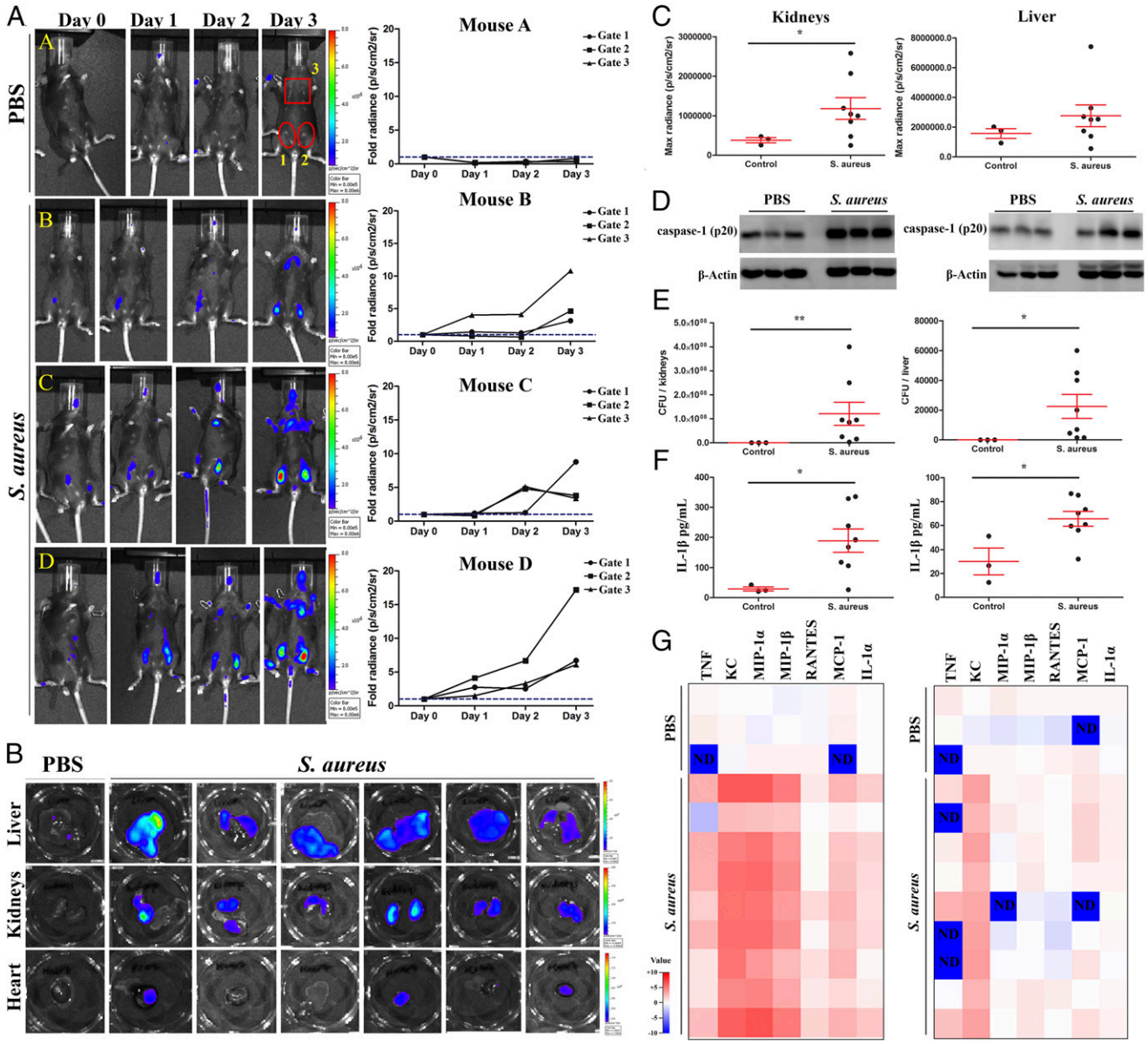

FIGURE 3. Caspase-1 biosensors are activated in *S. aureus*–infected mice. Representative IVIS images of caspase-1 biosensor mice infected with *S. aureus* or PBS day 0, 1, 2, and 3 after systemic infection (**A**). Regions of interest were drawn (red gates), and max radiance (p/s/cm^2/sr) was quantified. Data are expressed as fold max radiance relative to the max radiance detected in individual animals on day 0. IVIS images of tissues day 3 postinfection (**B**). Biosensor activation measured ex vivo in the kidneys and livers of control and infected mice (**C**). Tissues were homogenized and lysed for Western blot analysis of cleaved caspase-1 or β-actin (**D**). Western blot depicts caspase-1 activation in three control mice and three infected mice that exhibited the highest biosensor signal in the kidneys and livers (D). Homogenates were plated to enumerate bacterial CFU (**E**). Homogenates were centrifuged and supernatant was collected for CBA analysis (**F** and **G**). Heatmaps depict $\log_2$ fold change in cytokine/chemokine expression relative to the average of three control mice (G). Data shown are representative of three independent experiments (n = 7 PBS control and n = 25 WT *S. aureus*–infected animals). Data depicted in (C)–(G) are from one experiment (n = 3 PBS, n = 8 *S. aureus*–infected mice). *$p \leq 0.05$, **$p \leq 0.005$ by unpaired two-tailed t test (C–F).

(Fig. 4A–C, data not shown). To determine if biosensor activation corresponded to areas of caspase-1 activation in the colon, we isolated sections where we detected strong biosensor activation or control sections that exhibited little to no biosensor signal in the colons of mice treated with DSS. We detected activated caspase-1 specifically in areas of biosensor activation (Fig. 4D). We also found increased expression of inflammatory cytokines/chemokines, including IL-6, keratinocyte chemoattractant, IL-1β, and TNF, in the colons isolated from DSS-treated mice relative to the untreated controls (Fig. 4E). Together, these data demonstrate that the IQAD biosensor is activated early in the course of DSS-induced colitis in inflamed regions of the colon.

IQAD biosensors are activated in alloreactive donor cells during GVHD

Recently, caspase-1 activation has been reported to occur in immune cells of nonmyeloid origin during immune responses, including those occurring in models of autoimmune disease (20, 58–61). To determine if our sensor was activated in such contexts, we used an established model of GVHD. GVHD is a reaction that occurs following the transfer of donor immune cells (the graft) into an allogeneic host (62). Donor T cells recognize host alloantigens as foreign, leading to their activation and the production of proinflammatory cytokines and migration into host tissues including the skin, gastrointestinal tract, and liver (62–64).

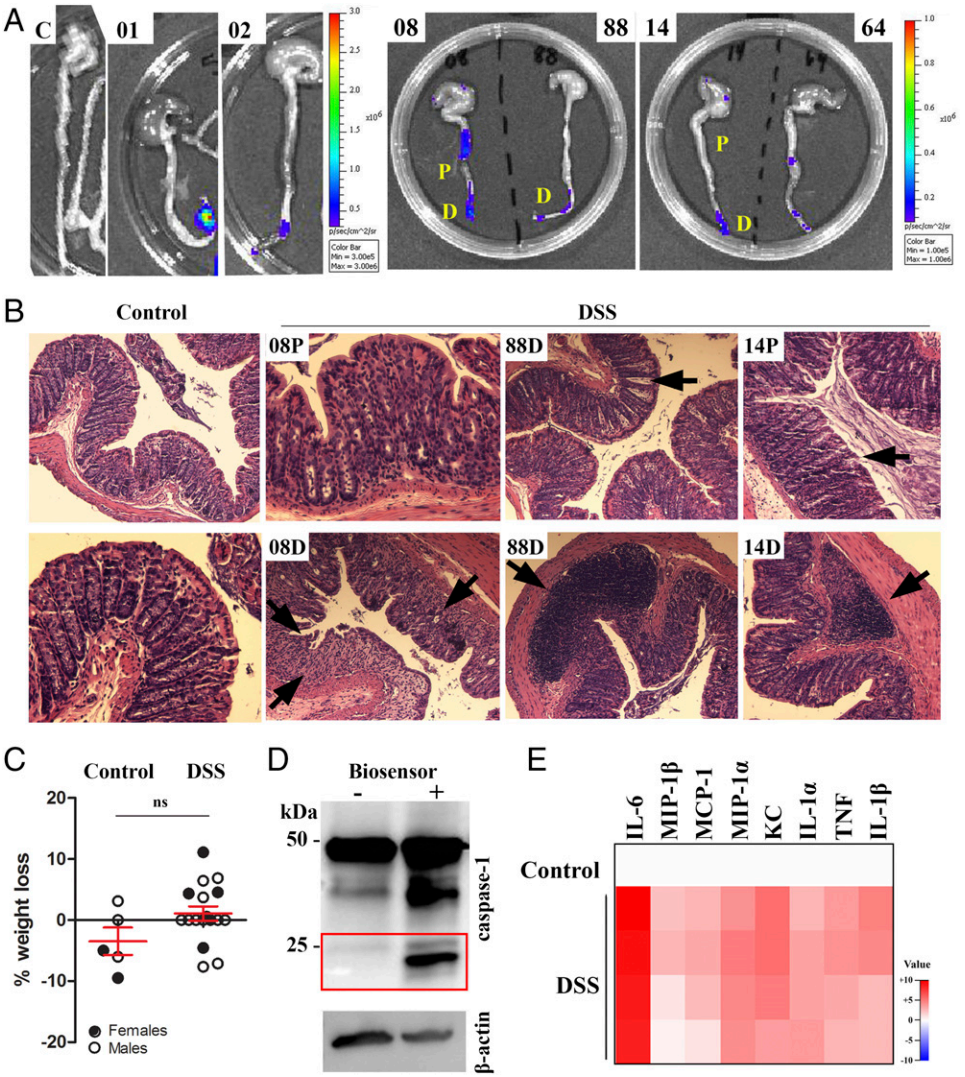

FIGURE 4. Caspase-1 biosensors are activated in inflamed areas of the colon during colitis. Representative IVIS images of caspase-1 biosensor male mice treated with DSS for 5 d (male control, DSS 01, DSS 02) and female mice treated with DSS for 7 d (female DSS 08, 88, 14, 64) (**A**). Tissue sections were acquired and histopathology was assessed. Representative images of histology sections obtained from the indicated mouse/region of the colon shown in (A), labeled with a P for proximal section or D for distal section (**B**). H&E stain of colons shown in (A), imaged at 40× magnification. Black arrows point to histopathological features of colitis including loss of crypts (08D, 88D), epithelial damage (08D), and inflammatory infiltration (88D, 14D), as well as crypt elongation (14P). Weight loss in male mice day 5 (white) or female mice day 7 (black) after DSS exposure (**C**). Tissue sections were isolated from regions of the colon where biosensor activation was detected (+) or control regions where no biosensor activation was detected DSS. Tissues were homogenized and lysed for Western blot analysis of cleaved caspase-1 or β-actin (**D**). Heatmaps depict $\log_2$ fold change in cytokine/chemokine expression in DSS mice relative to the average of two control mice (**E**). Data shown are representative of four independent experiments (n = 5 control and n = 17 DSS-treated mice). NS by unpaired two-tailed t test (C).

Inflammasome activation in T cells has been shown to contribute to the production of inflammatory cytokines (20, 58–61). We hypothesized that the biosensor would become activated in alloreactive donor T cells, and we could quantify bioluminescence in these cells and track their movement in the host over the course of disease. Furthermore, because the biosensor is only expressed in the donor cell population, we could specifically study donor-driven immune responses. To assess the IQAD biosensor in the context of GVHD, bone marrow cells and splenocytes were isolated from IQAD biosensor mice and transferred into irradiated WT C57BL/6 mice (syngeneic transfer) or BALB/c mice (allogeneic transfer). As a control, bone marrow cells only were transferred into irradiated allogeneic recipients, as this is necessary to reconstitute the host hematopoietic system but does not cause GVHD in mice (65–67). At various time points posttransfer, mice were imaged in vivo and bioluminescence was quantified. As expected, we found no biosensor activation in the syngeneic C57BL/6 mice or in the allogeneic BALB/c mice that received bone marrow cells only (Fig. 5A). However, robust biosensor signal was detected in vivo in BALB/c mice that received bone marrow cells and splenocytes (Fig. 5A). Biosensor signal first appeared in an area near the site of the spleen and over time, the signal spread to the abdomen. Mice were sacrificed on day 7 because of weight loss >20% in most animals. On day 7, prior to euthanasia, mice were imaged in vivo and then sacrificed, and biosensor activation was measured in tissues. We detected strong bioluminescence in the spleen and moderate signal in the intestines and mesenteric lymph nodes (Fig. 5B, 5C). By day 7, these mice exhibited increased clinical scores, as measured by decreased activity, hunched body posture, and lack of grooming, and had lost ∼20–25% of their body weight, indicative of acute GVHD (Fig. 5D, 5E). We also detected increased levels of cytokines and chemokines in the serum of GVHD mice, including TNF and IL-6 (data not shown). Although we are unable to determine if these cytokines/chemokines are donor or host derived, their presence in the serum is consistent with GVHD manifestation. To determine if the biosensor activation was occurring in donor T cells, T cells were isolated from IQAD mice by negative selection and transferred into syngeneic C57BL/6 CD45.1 recipient or allogeneic BALB/c mice. Mice were sacrificed 7 d after cell transfer, and biosensor activation was measured in vivo and ex vivo. As before, we detected biosensor activation in allogeneic recipient mice, specifically in the spleen, mesenteric lymph node, and small intestines (Supplemental Fig. 4A–C). We next isolated splenocytes and measured luciferase signal in vitro. We detected increased luciferase signal per cell in splenocytes isolated from allogeneic recipient mice compared with splenocytes isolated from the syngeneic control (Supplemental Fig. 4D). Flow cytometric analysis of these splenocytes revealed increased

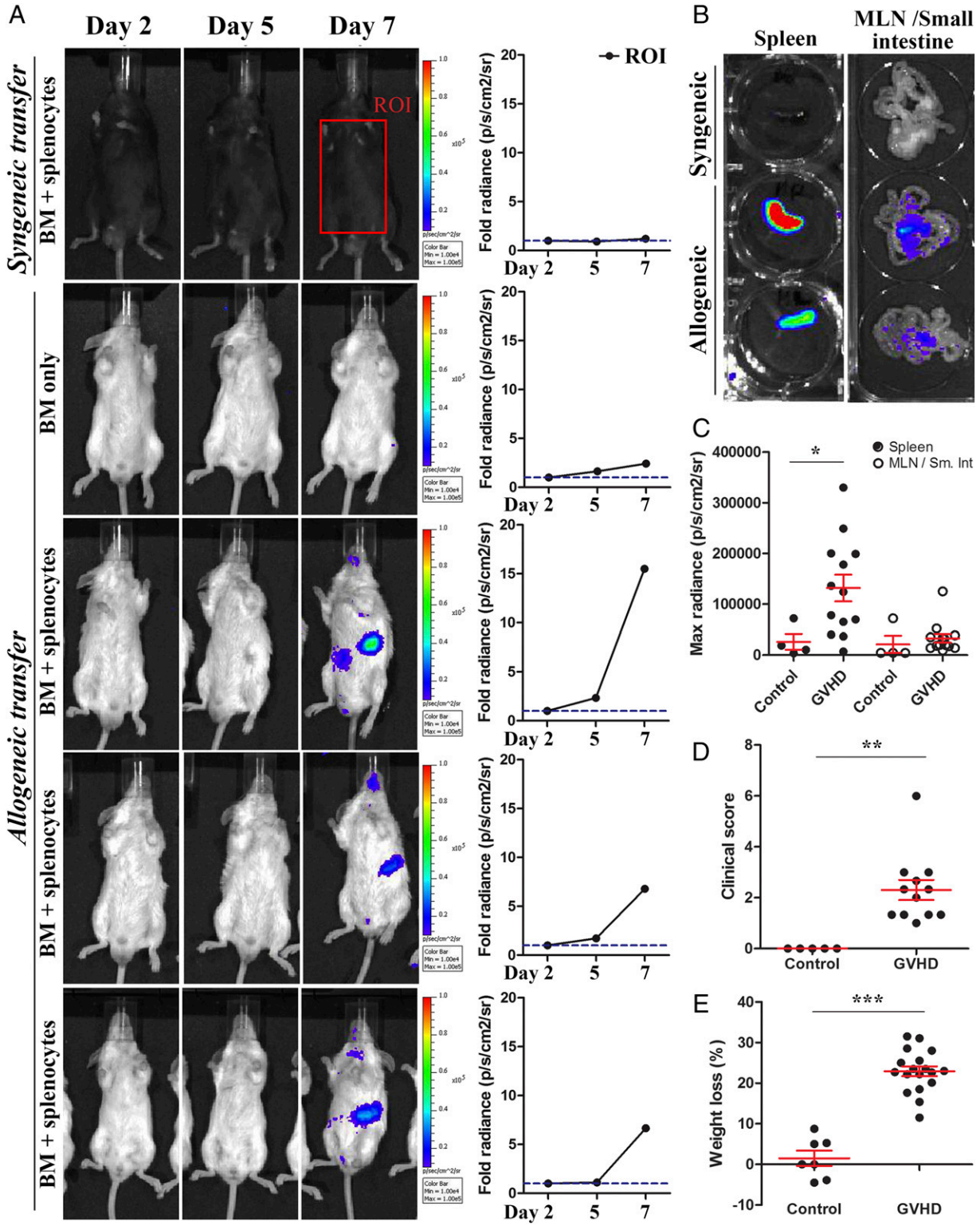

FIGURE 5. Biosensors are activated in alloreactive donor cells during GVHD. Bone marrow cells (10^7) ± 5×10^6 splenocytes from biosensor mice were transferred into irradiated C57BL/6 or BALB/c mice via i.v. injection. Representative IVIS images of mice at the indicated time points following syngeneic or allogeneic transfer of biosensor cells (**A**). Max radiance was quantified within the region of interest for each mouse and graphed as fold max radiance relative to the max radiance detected on day 2, after transfer of biosensor cells but prior to disease development (A). On day 7, tissues were harvested and biosensor activation was measured ex vivo in the spleen, mesenteric lymph node (MLN), and intestines (**B** and **C**). Clinical scores (**D**) and weight loss (**E**) were measured in control and GVHD mice. Error bars indicate mean ± SEM. Dots represent individual mice ($n = 4$ control, $n = 13$ GVHD) $^*p \leq 0.05$ (C), ($n = 5$ controls, $n = 12$ GVHD) $^{**}p \leq 0.005$ (D), and ($n = 7$ control, $n = 18$ GVHD), $^{***}p < 0.0005$ by unpaired two-tailed t test (E).

CD8 to CD4 T cell ratio and increased CD8 T cell activation in donor cells isolated from mice with GVHD (Supplemental Fig. 4E, 4F). Because all mice received the same donor cell population, collectively these data suggest that the IQAD biosensor is specifically activated in alloreactive T cells in mice with GVHD.

Discussion

In this study, we describe a bioluminescent sensor that quantitatively reports caspase-1 activation in cells and in living animals. We focused on caspase-1 because a diverse repertoire of PAMPs and DAMPs drive activation of a number of different inflammasomes, all of which culminate in the activation of caspase-1. The biosensor design was based on previously published circularly permuted luciferases that contain a protease recognition sequence between the two domains of the protein (21, 22, 68, 69). We hypothesized that if a caspase-1 target sequence was placed into the luciferase construct, then we would detect luciferase signal whenever caspase-1 was active in a cell. We initially screened a number of caspase-1 target sequences and identified the strongest luciferase signal in cells expressing the circularly permuted luciferase containing the IQAD target sequence from pro–caspase-7. Pro–caspase-7 is a well-established downstream target of caspase-1 (29–31, 70) and our data support this, as IQAD was cleaved in response to a variety of inflammatory stimuli in vitro and in vivo.

Our ultimate goal was to use caspse-1 biosensors to monitor inflammatory responses in vivo. To this end, we chose a *S. aureus* infection model of systemic inflammation and colitis model of tissue specific inflammation to validate our biosensor in living animals and tissues ex vivo. We detected bioluminescence that accumulated overtime in mice infected with *S. aureus* (Fig. 3). We also measured biosensor activation in tissues from *S. aureus*–infected mice and in the colons of mice with colitis (Figs. 3, 4). One caveat to using transgenic mice expressing IQAD biosensors is the level of background bioluminescence. These mice can exhibit up to $\sim 10^6$ p/s/cm^2/sr biosensor signal under normal conditions, with the highest signal occurring at the site of injection (tail or peritoneal cavity). In our experiments, we overcame this by quantifying the fold change in biosensor activation relative to the signal measured on day 0. However, background signal can be problematic when measuring small changes in bioluminescence in the abdomen area, as was the case with our colitis model. Additionally, detecting biosensor signal in vivo from certain tissues, like the kidneys, was difficult, because these organs are physically obstructed by other organs in the mouse. Despite the background signal in vivo, the ability to detect distinct areas of caspase-1 activation within tissues proved to be advantageous in our colitis model. Biosensor signal reliably identified colonic regions with increased inflammatory infiltration and loss of crypts in a model of DSS, which induced only moderate pathology observed in classical histopathological assessment and other experimental measurements of colitis (weight loss, colonic shortening, and Hemoccult) (Fig. 4). Notably, in both the *S. aureus* infection and colitis models, we detected active caspase-1 in tissues or regions of tissues that exhibited strong bioluminescence (Figs. 3, 4). These data highlight the potential of IQAD biosensor mice as guides to identifying locations in animals or within tissues where inflammatory responses are occurring.

We next wanted to evaluate the sensitivity of our biosensor using a stimulus or model of disease that does not induce robust inflammation. We speculated that because of the aforementioned high background in the IQAD biosensor mice, it would be very difficult to detect subtle changes in biosensor activation in these animals. However, if we transferred hematopoietic cells expressing the IQAD biosensor into irradiated WT mice, then we would be able to specifically monitor biosensor activation in immune cell populations in a WT host. To test this, we chose a model of acute GVHD. Our data demonstrate that the IQAD biosensor was activated in alloreactive T cells in specific tissues, primarily the spleen, in irradiated allogeneic recipient mice (Fig. 5, Supplemental Fig. 4). Donor cells were specifically activated in the context of GVHD, because little to no biosensor was detected in the allogeneic mice that received bone marrow cells only or in the syngeneic mice that received the same population of bone marrow cells and splenocytes. Accumulating evidence has supported a role for NLRP3 inflammasome and caspase-1 activation and IL-1β production in T cells (58, 61) and, more generally, in autoimmune diseases (20, 60). Martin et al. (59) recently reported a T cell–intrinsic inflammasome that drives production of IL-1β via NLRP3 and caspase-8. Pro–caspase-7 is a well-established target of caspase-8, so it is possible that caspase-8 is driving IQAD sensor activation in this model. Nevertheless, biosensor activation allowed the severity of disease to be readily monitored in this setting. The ability to monitor alloreactive T cell populations highlights the potential use of IQAD biosensors for monitoring T cell responses in the context of various autoimmune diseases.

We did observe substantial differences in the specificity of our IQAD sensor in response to inflammatory and apoptotic stimuli in vitro and in vivo. Although we observed that our biosensor was activated by apoptotic stimuli in vitro, sensor activation in these cells led to the release of the sensor into the supernatant, whereas the biosensor was retained in cells following treatment with inflammatory stimuli (Supplemental Fig. 3A). This is not entirely surprising, given the known degree of cross-talk between apoptotic and inflammatory caspase pathways (5, 71, 72). However, we did not observe sensor activation in the thymus where constitutively high levels of apoptosis are known to occur (Supplemental Fig. 3B). This is likely due to the fact that apoptotic cells are known to be cleared rapidly by tissue resident macrophages in vivo (41, 42) and/or biosensor degradation in the extracellular environment following release from apoptotic cells.

Despite this observation, our in vitro data suggest that corroborative evidence to discriminate between apoptotic and inflammatory caspase activation should be sought when possible, especially in model systems in which the mechanisms of pathogenesis are unknown.

In conclusion, we developed a bioluminescent reporter that detects caspase-1 activation. This biosensor is activated in response to a variety of inflammatory stimuli and murine models of human disease. Inflammation is a dynamic process, and the ability to track and quantify the initiation and onset of inflammatory responses in individual animals overtime has both experimental and economic value. Ultimately, we hope that this biosensor, when used concurrently with other conventional assays that measure inflammasome/caspase-1 activation, will help to identify novel sites of inflammation in animals and tissues, which may facilitate the development and evaluation of future therapies for inflammatory diseases.

Acknowledgments

We thank Jessica Mattick for assisting with the generation of heatmaps using Rstudio. We thank Pi-Chen Yam (Loyola University Chicago) for assisting with the GVHD studies.

Disclosures

E.M.C., S.T., and M.W. have interest in a provisional U.S. patent, "Caspase-1 Biosensors, Transgenic Mouse Expressing The Same And Methods Of Monitoring Inflammatory Diseases," under serial no. 62/688,627. The other authors have no financial conflicts of interest.

References

1. Sharma, D., and T. D. Kanneganti. 2016. The cell biology of inflammasomes: mechanisms of inflammasome activation and regulation. *J. Cell Biol.* 213: 617–629.
2. Vanaja, S. K., V. A. Rathinam, and K. A. Fitzgerald. 2015. Mechanisms of inflammasome activation: recent advances and novel insights. *Trends Cell Biol.* 25: 308–315.

3. Guo, H., J. B. Callaway, and J. P. Ting. 2015. Inflammasomes: mechanism of action, role in disease, and therapeutics. *Nat. Med.* 21: 677–687.
4. Sollberger, G., G. E. Strittmatter, M. Garstkiewicz, J. Sand, and H. D. Beer. 2014. Caspase-1: the inflammasome and beyond. *Innate Immun.* 20: 115–125.
5. Man, S. M., and T. D. Kanneganti. 2016. Converging roles of caspases in inflammasome activation, cell death and innate immunity. *Nat. Rev. Immunol.* 16: 7–21.
6. Stewart, M. K., and B. T. Cookson. 2016. Evasion and interference: intracellular pathogens modulate caspase-dependent inflammatory responses. *Nat. Rev. Microbiol.* 14: 346–359.
7. Place, D. E., and T. D. Kanneganti. 2018. Recent advances in inflammasome biology. *Curr. Opin. Immunol.* 50: 32–38.
8. Denes, A., G. Lopez-Castejon, and D. Brough. 2012. Caspase-1: is IL-1 just the tip of the ICEberg? *Cell Death Dis.* 3: e338.
9. Strowig, T., J. Henao-Mejia, E. Elinav, and R. Flavell. 2012. Inflammasomes in health and disease. *Nature* 481: 278–286.
10. Latz, E., T. S. Xiao, and A. Stutz. 2013. Activation and regulation of the inflammasomes. *Nat. Rev. Immunol.* 13: 397–411.
11. Broz, P., and V. M. Dixit. 2016. Inflammasomes: mechanism of assembly, regulation and signalling. *Nat. Rev. Immunol.* 16: 407–420.
12. Franchi, L., R. Muñoz-Planillo, and G. Núñez. 2012. Sensing and reacting to microbes through the inflammasomes. *Nat. Immunol.* 13: 325–332.
13. Cullen, S. P., C. J. Kearney, D. M. Clancy, and S. J. Martin. 2015. Diverse activators of the NLRP3 inflammasome promote IL-1β secretion by triggering necrosis. *Cell Rep.* 11: 1535–1548.
14. He, Y., H. Hara, and G. Núñez. 2016. Mechanism and regulation of NLRP3 inflammasome activation. *Trends Biochem. Sci.* 41: 1012–1021.
15. Walsh, J. G., D. A. Muruve, and C. Power. 2014. Inflammasomes in the CNS. *Nat. Rev. Neurosci.* 15: 84–97.
16. de Torre-Minguela, C., P. Mesa Del Castillo, and P. Pelegrín. 2017. The NLRP3 and pyrin inflammasomes: implications in the pathophysiology of autoinflammatory diseases. *Front. Immunol.* 8: 43.
17. Poeck, H., M. Bscheider, O. Gross, K. Finger, S. Roth, M. Rebsamen, N. Hannesschläger, M. Schlee, S. Rothenfusser, W. Barchet, et al. 2010. Recognition of RNA virus by RIG-I results in activation of CARD9 and inflammasome signaling for interleukin 1 beta production. [Published erratum appears in 2014 *Nat. Immunol.* 15: 109.] *Nat. Immunol.* 11: 63–69.
18. Xu, H., J. Yang, W. Gao, L. Li, P. Li, L. Zhang, Y. N. Gong, X. Peng, J. J. Xi, S. Chen, et al. 2014. Innate immune sensing of bacterial modifications of Rho GTPases by the Pyrin inflammasome. *Nature* 513: 237–241.
19. Deswaerte, V., S. M. Ruwanpura, and B. J. Jenkins. 2017. Transcriptional regulation of inflammasome-associated pattern recognition receptors, and the relevance to disease pathogenesis. *Mol. Immunol.* 86: 3–9.
20. Zhao, C., Y. Gu, X. Zeng, and J. Wang. 2018. NLRP3 inflammasome regulates Th17 differentiation in rheumatoid arthritis. *Clin. Immunol.* 197: 154–160.
21. Fan, F., B. F. Binkowski, B. L. Butler, P. F. Stecha, M. K. Lewis, and K. V. Wood. 2008. Novel genetically encoded biosensors using firefly luciferase. *ACS Chem. Biol.* 3: 346–351.
22. Galbán, S., Y. H. Jeon, B. M. Bowman, J. Stevenson, K. A. Sebolt, L. M. Sharkey, M. Lafferty, B. A. Hoff, B. L. Butler, S. S. Wigdal, et al. 2013. Imaging proteolytic activity in live cells and animal models. *PLoS One* 8: e66248.
23. Dreier, R. F., J. C. Santos, and P. Broz. 2018. Detecting release of bacterial dsDNA into the host cytosol using fluorescence microscopy. *Methods Mol. Biol.* 1714: 199–213.
24. O'Doherty, U., W. J. Swiggard, and M. H. Malim. 2000. Human immunodeficiency virus type 1 spinoculation enhances infection through virus binding. *J. Virol.* 74: 10074–10080.
25. Paik, W., F. Alonzo, III, and K. L. Knight. 2018. Probiotic exopolysaccharide protects against systemic *Staphylococcus aureus* infection, inducing dual-functioning macrophages that restrict bacterial growth and limit inflammation. *Infect. Immun.* 87.
26. Grayczyk, J. P., C. J. Harvey, I. Laczkovich, and F. Alonzo, III. 2017. A lipoylated metabolic protein released by Staphylococcus aureus suppresses macrophage activation. *Cell Host Microbe* 22: 678–687.e9.
27. Alonzo, F., III, M. A. Benson, J. Chen, R. P. Novick, B. Shopsin, and V. J. Torres. 2012. *Staphylococcus aureus* leucocidin ED contributes to systemic infection by targeting neutrophils and promoting bacterial growth in vivo. *Mol. Microbiol.* 83: 423–435.
28. Cannon, A. R., P. V. Kuprys, A. N. Cobb, X. Ding, A. N. Kothari, P. C. Kuo, J. M. Eberhardt, A. M. Hammer, N. L. Morris, X. Li, and M. A. Choudhry. 2018. Alcohol enhances symptoms and propensity for infection in inflammatory bowel disease patients and a murine model of DSS-induced colitis. *J. Leukoc. Biol.* 104: 543–555.
29. Lamkanfi, M., and T. D. Kanneganti. 2010. Caspase-7: a protease involved in apoptosis and inflammation. *Int. J. Biochem. Cell Biol.* 42: 21–24.
30. Boucher, D., V. Blais, M. Drag, and J. B. Denault. 2011. Molecular determinants involved in activation of caspase 7. *Biosci. Rep.* 31: 283–294.
31. Lamkanfi, M., T. D. Kanneganti, P. Van Damme, T. Vanden Berghe, I. Vanoverberghe, J. Vandekerckhove, P. Vandenabeele, K. Gevaert, and G. Núñez. 2008. Targeted peptidecentric proteomics reveals caspase-7 as a substrate of the caspase-1 inflammasomes. *Mol. Cell. Proteomics* 7: 2350–2363.
32. Riedl, S. J., P. Fuentes-Prior, M. Renatus, N. Kairies, S. Krapp, R. Huber, G. S. Salvesen, and W. Bode. 2001. Structural basis for the activation of human procaspase-7. *Proc. Natl. Acad. Sci. USA* 98: 14790–14795.
33. Bartok, E., F. Bauernfeind, M. G. Khaminets, C. Jakobs, B. Monks, K. A. Fitzgerald, E. Latz, and V. Hornung. 2013. iGLuc: a luciferase-based inflammasome and protease activity reporter. *Nat. Methods* 10: 147–154.
34. Compan, V., A. Baroja-Mazo, L. Bragg, A. Verkhratsky, J. Perroy, and P. Pelegrin. 2012. A genetically encoded IL-1β bioluminescence resonance energy transfer sensor to monitor inflammasome activity. *J. Immunol.* 189: 2131–2137.
35. Hornung, V., A. Ablasser, M. Charrel-Dennis, F. Bauernfeind, G. Horvath, D. R. Caffrey, E. Latz, and K. A. Fitzgerald. 2009. AIM2 recognizes cytosolic dsDNA and forms a caspase-1-activating inflammasome with ASC. *Nature* 458: 514–518.
36. Franchi, L., T. Eigenbrod, R. Muñoz-Planillo, U. Ozkurede, Y. G. Kim, C. Arindam, M. Gale, Jr., R. H. Silverman, M. Colonna, S. Akira, and G. Núñez. 2014. Cytosolic double-stranded RNA activates the NLRP3 inflammasome via MAVS-induced membrane permeabilization and K+ efflux. *J. Immunol.* 193: 4214–4222.
37. Fernandes-Alnemri, T., J. W. Yu, P. Datta, J. Wu, and E. S. Alnemri. 2009. AIM2 activates the inflammasome and cell death in response to cytoplasmic DNA. *Nature* 458: 509–513.
38. Liu, C. 2013. Strategies for designing transgenic DNA constructs. *Methods Mol. Biol.* 1027: 183–201.
39. Powell, S. K., R. Rivera-Soto, and S. J. Gray. 2015. Viral expression cassette elements to enhance transgene target specificity and expression in gene therapy. *Discov. Med.* 19: 49–57.
40. Abe, T., and T. Fujimori. 2013. Reporter mouse lines for fluorescence imaging. *Dev. Growth Differ.* 55: 390–405.
41. Dzhagalov, I. L., K. G. Chen, P. Herzmark, and E. A. Robey. 2013. Elimination of self-reactive T cells in the thymus: a timeline for negative selection. *PLoS Biol.* 11: e1001566.
42. Elliott, M. R., and K. S. Ravichandran. 2016. The dynamics of apoptotic cell clearance. *Dev. Cell* 38: 147–160.
43. Centers for Disease Control and Prevention. 2011. *Staphyloccocus aureus* in healthcare settings. Available at: https://www.cdc.gov/hai/organisms/staph.html. Accessed: September 17, 2019.
44. Powers, M. E., and J. Bubeck Wardenburg. 2014. Igniting the fire: *Staphylococcus aureus* virulence factors in the pathogenesis of sepsis. *PLoS Pathog.* 10: e1003871.
45. Alonzo, F., III, and V. J. Torres. 2013. Bacterial survival amidst an immune onslaught: the contribution of the *Staphylococcus aureus* leukotoxins. *PLoS Pathog.* 9: e1003143.
46. Miller, L. S., and J. S. Cho. 2011. Immunity against *Staphylococcus aureus* cutaneous infections. *Nat. Rev. Immunol.* 11: 505–518.
47. Melehani, J. H., and J. A. Duncan. 2016. Inflammasome activation can mediate tissue-specific pathogenesis or protection in *Staphylococcus aureus* infection. *Curr. Top. Microbiol. Immunol.* 397: 257–282.
48. Holzinger, D., L. Gieldon, V. Mysore, N. Nippe, D. J. Taxman, J. A. Duncan, P. M. Broglie, K. Marketon, J. Austermann, T. Vogl, et al. 2012. *Staphylococcus aureus* Panton-Valentine leukocidin induces an inflammatory response in human phagocytes via the NLRP3 inflammasome. *J. Leukoc. Biol.* 92: 1069–1081.
49. Craven, R. R., X. Gao, I. C. Allen, D. Gris, J. Bubeck Wardenburg, E. McElvania-Tekippe, J. P. Ting, and J. A. Duncan. 2009. *Staphylococcus aureus* alpha-hemolysin activates the NLRP3-inflammasome in human and mouse monocytic cells. *PLoS One* 4: e7446.
50. Kebaier, C., R. R. Chamberland, I. C. Allen, X. Gao, P. M. Broglie, J. D. Hall, C. Jania, C. M. Doerschuk, S. L. Tilley, and J. A. Duncan. 2012. Staphylococcus aureus α-hemolysin mediates virulence in a murine model of severe pneumonia through activation of the NLRP3 inflammasome. *J. Infect. Dis.* 205: 807–817.
51. Muñoz-Planillo, R., L. Franchi, L. S. Miller, and G. Núñez. 2009. A critical role for hemolysins and bacterial lipoproteins in *Staphylococcus aureus*-induced activation of the Nlrp3 inflammasome. *J. Immunol.* 183: 3942–3948.
52. Mariathasan, S., D. S. Weiss, K. Newton, J. McBride, K. O'Rourke, M. Roose-Girma, W. P. Lee, Y. Weinrauch, D. M. Monack, and V. M. Dixit. 2006. Cryopyrin activates the inflammasome in response to toxins and ATP. *Nature* 440: 228–232.
53. Błażejewski, A. J., S. Thiemann, A. Schenk, M. C. Pils, E. J. C. Gálvez, U. Roy, U. Heise, M. R. de Zoete, R. A. Flavell, and T. Strowig. 2017. Microbiota normalization reveals that canonical caspase-1 activation exacerbates chemically induced intestinal inflammation. *Cell Rep.* 19: 2319–2330.
54. Siegmund, B., H. A. Lehr, G. Fantuzzi, and C. A. Dinarello. 2001. IL-1 beta -converting enzyme (caspase-1) in intestinal inflammation. *Proc. Natl. Acad. Sci. USA* 98: 13249–13254.
55. Gagliani, N., N. W. Palm, M. R. de Zoete, and R. A. Flavell. 2014. Inflammasomes and intestinal homeostasis: regulating and connecting infection, inflammation and the microbiota. *Int. Immunol.* 26: 495–499.
56. Bábíčková, J., Ľ. Tóthová, E. Lengyelová, A. Bartoňová, J. Hodosy, R. Gardlík, and P. Celec. 2015. Sex differences in experimentally induced colitis in mice: a role for estrogens. *Inflammation* 38: 1996–2006.
57. Chassaing, B., J. D. Aitken, M. Malleshappa, and M. Vijay-Kumar. 2014. Dextran sulfate sodium (DSS)-induced colitis in mice. *Curr. Protoc. Immunol.* 104: Unit 15.25.
58. Arbore, G., E. E. West, R. Spolski, A. A. B. Robertson, A. Klos, C. Rheinheimer, P. Dutow, T. M. Woodruff, Z. X. Yu, L. A. O'Neill, et al. 2016. T helper 1 immunity requires complement-driven NLRP3 inflammasome activity in $CD4^+$ T cells. *Science* 352: aad1210.
59. Martin, B. N., C. Wang, C. J. Zhang, Z. Kang, M. F. Gulen, J. A. Zepp, J. Zhao, G. Bian, J. S. Do, B. Min, et al. 2016. T cell-intrinsic ASC critically promotes T(H)17-mediated experimental autoimmune encephalomyelitis. *Nat. Immunol.* 17: 583–592.
60. Zhao, J., H. Wang, C. Dai, H. Wang, H. Zhang, Y. Huang, S. Wang, F. Gaskin, N. Yang, and S. M. Fu. 2013. P2X7 blockade attenuates murine lupus nephritis by inhibiting activation of the NLRP3/ASC/caspase 1 pathway. *Arthritis Rheum.* 65: 3176–3185.

61. Doitsh, G., N. L. Galloway, X. Geng, Z. Yang, K. M. Monroe, O. Zepeda, P. W. Hunt, H. Hatano, S. Sowinski, I. Muñoz-Arias, and W. C. Greene. 2014. Cell death by pyroptosis drives CD4 T-cell depletion in HIV-1 infection. [Published erratum appears in 2017 *Nature* 544: 124.] *Nature* 505: 509–514.
62. Zeiser, R., and B. R. Blazar. 2017. Acute graft-versus-host disease - biologic process, prevention, and therapy. *N. Engl. J. Med.* 377: 2167–2179.
63. Malard, F., B. Gaugler, B. Lamarthee, and M. Mohty. 2016. Translational opportunities for targeting the Th17 axis in acute graft-vs.-host disease. *Mucosal Immunol.* 9: 299–308.
64. Holtan, S. G., M. Pasquini, and D. J. Weisdorf. 2014. Acute graft-versus-host disease: a bench-to-bedside update. *Blood* 124: 363–373.
65. Edinger, M., P. Hoffmann, J. Ermann, K. Drago, C. G. Fathman, S. Strober, and R. S. Negrin. 2003. CD4+CD25+ regulatory T cells preserve graft-versus-tumor activity while inhibiting graft-versus-host disease after bone marrow transplantation. *Nat. Med.* 9: 1144–1150.
66. Schroeder, M. A., K. Ashami, and K. Staser. 2018. Modeling chronic graft versus host disease in mice using allogeneic bone marrow and splenocyte transfer. *Curr. Protoc. Pharmacol.* 83: e47.
67. Cohen, J. L., O. Boyer, B. Salomon, R. Onclercq, F. Charlotte, S. Bruel, G. Boisserie, and D. Klatzmann. 1997. Prevention of graft-versus-host disease in mice using a suicide gene expressed in T lymphocytes. *Blood* 89: 4636–4645.
68. Wigdal, S. S., J. L. Anderson, G. J. Vidugiris, J. Shultz, K. V. Wood, and F. Fan. 2008. A novel bioluminescent protease assay using engineered firefly luciferase. *Curr. Chem. Genomics* 2: 16–28.
69. Kilianski, A., A. M. Mielech, X. Deng, and S. C. Baker. 2013. Assessing activity and inhibition of Middle East respiratory syndrome coronavirus papain-like and 3C-like proteases using luciferase-based biosensors. *J. Virol.* 87: 11955–11962.
70. Agard, N. J., D. Maltby, and J. A. Wells. 2010. Inflammatory stimuli regulate caspase substrate profiles. *Mol. Cell. Proteomics* 9: 880–893.
71. Creagh, E. M. 2014. Caspase crosstalk: integration of apoptotic and innate immune signalling pathways. *Trends Immunol.* 35: 631–640.
72. Taabazuing, C. Y., M. C. Okondo, and D. A. Bachovchin. 2017. Pyroptosis and apoptosis pathways engage in bidirectional crosstalk in monocytes and macrophages. *Cell Chem. Biol.* 24: 507–514.e4